https://www.imavs.org/pdf/imav.2017.23

Simulation and Control of a Tandem Tiltwing RPAS Without Experimental Data

Y. Beyer*, T. Krüger, A. Krüger, M. Steen, P. Hecker
Institute of Flight Guidance, TU Braunschweig, Hermann-Blenk-Str. 27, 38108 Brunswick, Germany

ABSTRACT

The tandem tiltwing is one of many aircraft configurations providing vertical takeoff and landing (VTOL). This configuration is expected to be especially suitable for missions requiring VTOL capability combined with high range and space for payload. In this article, an overview of the simulation process of a tandem tiltwing remotely piloted aircraft system (RPAS) without experimental data and its control is given. Contrary to custom, the flight dynamic model, especially the whole aerodynamics model, consists of theoretical equations and interpolations depending on estimated parameters. Compared to complex wind tunnel tests, this approach is less expensive. In order to stabilize the unstable flight characteristics of the tandem tiltwing, a linear-quadratic regulator (LQR) is designed. As the change of operating point of this VTOL aircraft is significant, the LQR has to be gain scheduled. For that, multiple trim points during the transition are ascertained making a controlled transition possible. However, due to the lack of test data, the probability of failure caused by an inaccurate flight controller relying on the flight dynamic model is increased. Hence, a robustness analysis of the closed-loop system is conducted, where the probability of stability of the closed-loop real RPAS is estimated by a Monte Carlo method. For this purpose, all uncertain model parameters are changed based on the normal distribution by defining their standard deviation.

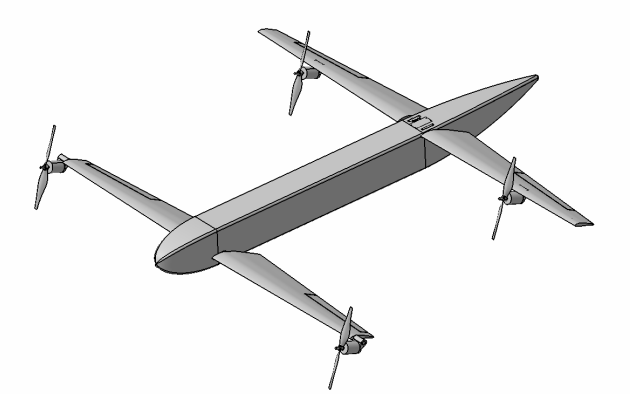

Figure 1: CAD model of the tandem tiltwing

List of Symbols

α	angle of attack
β	sideslip angle
ϑ_1	front wing's tilt angle
ϑ_2	aft wing's tilt angle
ω_i	angular velocity of motor i
$\Phi,\ \Theta,\ \Psi$	Euler angles
b	span
C_D	drag coefficient
C_l	rolling moment coefficient
C_L	lift coefficient
C_m	pitching moment coefficient
C_n	yawing moment coefficient
D	drag
$\boldsymbol{e}$	error vector
L	lift
p	roll rate
P	power
q	pitch rate
Q	lateral force
r	yaw rate
$\boldsymbol{r}$	reference command vector
T	thrust
u	velocity in x direction
$\boldsymbol{u}$	input vector
v	velocity in y direction
w	velocity in z direction
$\boldsymbol{x}$	state vector

List of Indices

η_i	elevon i
ϑ_i	tilt angle i
ω_i	motor i
$b,\ t_i,\ c,\ g,\ w$	coordinate systems

Meaning of Exponents

cm/W	cm relative to the wind (W); example

*Email address: y.beyer@tu-bs.de

http://www.imavs.org/

http://www.imavs.org/

1 INTRODUCTION

The tandem tiltwing RPAS [1], which is shown in figure 1, is a VTOL aircraft that is controlled like a quadcopter during hover and like a tandem wing during cruise. In similar projects, this configuration is also called quad tiltwing [2, 3, 4] and [5, 6]. It displays some advantages compared to other VTOL airplanes. The span is decreased maintaining the same aspect ratio and consequently the same aerodynamic efficiency resulting in a more compact aircraft. Moreover, the possibility of a relatively large displacement of the center of mass is likewise convenient. Four motors are directly attached to the wings providing a quadcopter configuration in hover mode. Additionally, there are a few advantages compared to a tilt*rotor* configuration, such as the propeller stream is not blocked by the wings and that only two (larger) tilt mechanisms are needed instead of four. Also, a simple trimming possibility is provided by the tiltwings. However, the realization of a tandem tiltwing is relatively complicated due to the two tilt mechanisms carrying the moment of both wings and motors as well as the detached flow on the upper side of the wings during the transition.

Static longitudinal stability of a tandem wing is accomplished by a higher loading of the front wing. However, as a higher loading of the front wing usually decreases efficiency, the loading of both wings should be similar causing static longitudinal instability. Since the motors are used for quadcopter control, they can similarly be used for yaw control during cruise. That makes a rudder as well as vertical stabilizer unnecessary so that they are consequently omitted in order to make the aircraft more lightweight. Thus, the tandem tiltwing displays lateral-directional instability.

The tandem tiltwing can be controlled by the four motors, both tilt angles as well as two elevons. Elevons act as both elevators and ailerons. They are located at the front wing because of higher sensitivity. As the control of the unstable and unsteady flight dynamics of the presented VTOL are very challenging, a high accuracy of the flight dynamics model is crucial in order to properly design an attitude controller. However, no wind tunnel test data is available. Instead, the aerodynamics are calculated by formulas and interpolations covering the complete domain of the angle of attack and the sideslip angle as well as effects depending on the angular rates of the aircraft and wing interaction considering a delayed downwash of the front wing.

Some technical data of the presented tandem tiltwing RPAS is listed in tabular 1.

2 FLIGHT DYNAMIC MODEL

In this section the analytical flight dynamic model of the tandem tiltwing is described. Figure 13 shows an outline of the tandem tiltwing and the needed coordinate systems.

category	value/product
mass	$5\,\mathrm{kg}$
design airspeed	$20\,\mathrm{m\,s^{-1}}$
measures	$1.4\,\mathrm{m} \times 1.4\,\mathrm{m} \times 0.3\,\mathrm{m}$
propellers	$4\times$ AeroNau 10x5
motors	$4\times$ AXI $2826/10$ (V2)
ESCs	$4\times$ ZTW Spider Series 50A OPTO 2˜6
batteries	$2\times$ Turinigy $5000\,\mathrm{mA\,h}$ 5S 25C LiPo

Table 1: Technical data of the tandem tiltwing RPAS.

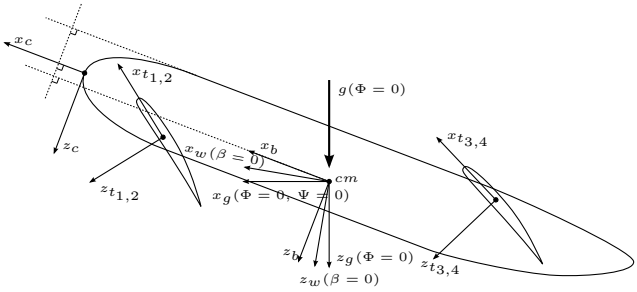

Figure 2: Two-dimensional illustration of the used coordinate systems to simulate the tandem tiltwing. In the general case, x_w, z_w, x_g, z_g and g are three-dimensional in this side view.

2.1 Motor and Actuator Dynamics

The motor dynamics are based on a first order delay [7] using the motor torque constant, the inertia as well as the internal resistance as parameters. The tilt servos and elevon servos are modeled as second order delays estimating a damping ratio and frequency.

2.2 Propeller Aerodynamics and Dynamics

The propeller thrust and power are calculated with aid of a map provided by [8]. The map depends on the angular velocity as well as the vertical airspeed as it is shown in figure 3 and 4. The following moments and forces are considered [9]:

- thrust vector,
- moment vector due to lever arms,

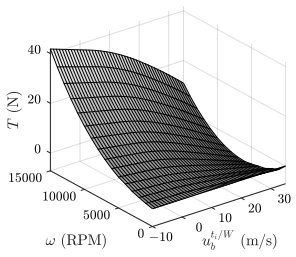

Figure 3: Propeller thrust.

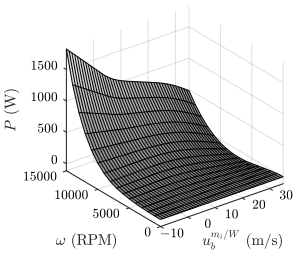

Figure 4: Propeller power.

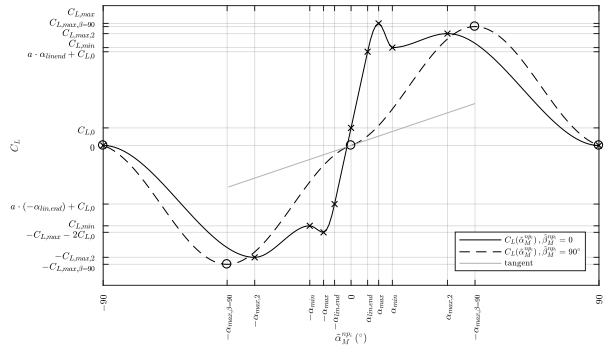

Figure 5: Lift coefficient as a function of the modified angle of attack seen by the tiltwing obtained by interpolation of characteristic points.

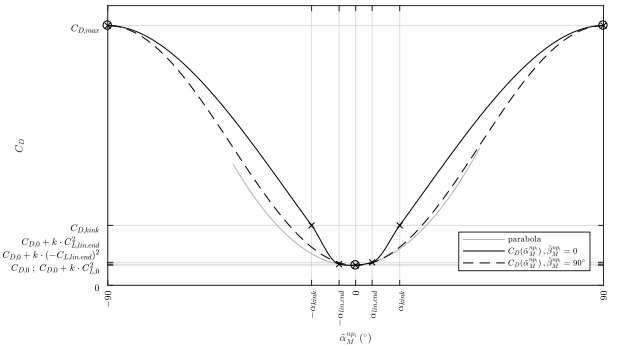

Figure 6: Drag coefficient as a function of the modified angle of attack seen by the tiltwing obtained by interpolation of characteristic points.

- moment vector due to drag,
- moment vector due to inertia when accelerated,
- moment vector due to the propeller gyro effect.

2.3 Fuselage and Wing Aerodynamics

Lift and drag coefficient interpolation. Since the range of the appearing angle of attack is large (it ranges at least from $0°$ to $90°$), the modeling of nonlinear effects is required. The most important aerodynamic coefficients, the lift coefficient C_L and the drag coefficient C_D, must inevitably be defined with respect to the complete range of the angle of attack which is quite uncertain without experimental data. Moreover, at low speed and high wind velocities, the sideslip angle can become large, too. Consequently, the lift coefficient (figure 5) and the drag coefficient (figure 6) must be a nonlinear function with respect to the whole range of the sideslip angle. According to the definition, the angle of attack is defined in the range of $-180° \leq \alpha \leq 180°$ while the sideslip angle is defined in the range of $-90° \leq \beta \leq 90°$. However, working with high angles of attack and sideslip angles a reversed definition of the ranges is desirable. That is why, in this work, a modified angle of attack α_M and a modified sideslip angle β_M are defined changing the order of rotation (appendix 20). For small aerodynamic angles, the difference between the original aerodynamic angles and the modified angles is negligible.

The functions of the lift coefficient as well as the drag coefficient are created by cubic spline interpolation stepwise in between of two points whose slope is known. The points are selected as characteristic points based on experimental data of similar projects [5, 10] as well as literature [11]. Because of the uncertainty of the points in the nonlinear area, all points are defined as parameters which will be changed randomly in the robustness analysis.

Local aerodynamics. There are multiple additional crucial aerodynamic coefficients such as the moment coefficients. Usually, these coefficients are determined by wind tunnel experiments or linear mathematical approaches are used. The linear approaches work with constant aerodynamic derivatives, which are the dimensionless partial derivatives of aerodynamic coefficients with respect to one state, output element or input element. However, for a tiltwing, a linear approach does not seem suitable. That is why a different approach is used.

Except for the lift coefficient, the drag coefficient and the fuselage aerodynamic coefficients, no other aerodynamic coefficients are defined directly. As there are convenient formulas to calculate the fuselage moments, this is done separately. The aerodynamic moments produced by the wings are calculated by the aerodynamic forces acting on movable centers of pressure, thus, acting on lever arms. That means, the aircraft is divided into five parts (left front wing, right front wing, right aft wing, left aft wing and fuselage) whose aerodynamics are calculated independently. Then, the force and moment vector in the cm of the aircraft is calculated by multiplying the local force vectors with the current lever arms to the centers of pressure and summarizing the result including the aerodynamics of the fuselage.

Wing interaction. Until this point all aerodynamic components of the tandem tiltwing were treated independently. Indeed, there is an interaction between the aerodynamic components as well as the propellers. The modeled interaction is restricted to a lift coefficient dependent and delayed downwash of the front wing decreasing the angle of attack of the aft wing according to [11].

2.4 Summary of Assumptions

The complexity of the reality can barely be modeled. The following assumptions of the model may cause substantial deviations of the model and the reality:

- the structure of the aircraft is rigid,
- no interaction between the propellers, the wings and the fuselage except of a simple downwash model,

http://www.imavs.org/

http://www.imavs.org/

- no noncontinuous phenomenons e.g. for the lift coefficient or the actuators,
- no dependency of the aerodynamics on the Reynolds number and Mach number,
- the thrust does not depend on the lateral velocity seen from the propeller.

3 STABILITY AND CONTROL

In this section, the stability of the tandem tiltwing is analyzed by means of the indirectly defined aerodynamic derivatives as well as root loci. For these linear methods, the model has to be linearized in the first place. Based on the obtained linear models, a gain scheduled LQR is designed.

3.1 Operating Points and Linearization

As the desired control strategy requires a linear model, the flight dynamic model has to be linearized in multiple operating points. At first, these operating points have to be found starting with steady-state operating points. Therefore, all steady states are defined and if known, the value also is defined. This is done by changing the front tilt angle in the following steps:

$$\begin{aligned}\vartheta_1(^\circ) = (\ & 90 \quad 80 \quad 70 \quad 60 \quad 50 \quad 40 \quad 30 \quad 20 \\ & 14 \quad 10 \quad 7 \quad 3\ )\ .\end{aligned} \tag{1}$$

The outcome is the input vector as well as the airspeed. In the next step, for all obtained airspeeds an additional trimming for a forward acceleration of $\mathrm{d}u_b^{cm/W}/\mathrm{d}t = 3\,\mathrm{m\,s^{-2}}$ as well as a deceleration of $\mathrm{d}u_b^{cm/W}/\mathrm{d}t = -3\,\mathrm{m\,s^{-2}}$ is conducted. While the forward acceleration is easy to trim, the demanded deceleration can not be achieved in horizontal flight. That is why a vertical speed is allowed for the deceleration in order to convert kinetic energy to potential energy. The outcome of the unsteady trimming is the input vector.

3.2 Open-Loop Stability

The static stability calculations can be split into longitudinal static stability and lateral-directional static stability.

Longitudinal static stability. A negative slope of the pitching moment coefficient with respect to the angle of attack is the most important condition for longitudinal static stability. The corresponding illustration is shown in figure 7 varying the relative center of mass (cm) position $0 \leq h \leq 1$ which is zero at the neutral point of the front wing and one at the neutral point of the aft wing. According to the figure, the longitudinal motion of the tandem tiltwing becomes unstable if $h \geq 0.46$. However, because of efficiency purposes $h = 0.5$, which causes static instability, is desired. In figure 8, the pitch damping is illustrated. Small angles of attack lead to a large pitch damping, while the positive slope of the curve corresponding to $\vartheta_1 = 14^\circ$ causes unstable pitch damping.

Lateral-directional static stability. The conditions of lateral-directional static stability mainly are a negative slope of the rolling moment coefficient (figure 9) and a positive slope of the yawing moment coefficient (figure 10) with respect to the sideslip angle. However, the yawing moment is unstable because the unstable moment produced by the fuselage is not overcompensated by a vertical stabilizer. The other stability derivatives depending on the rates were investigated equally.

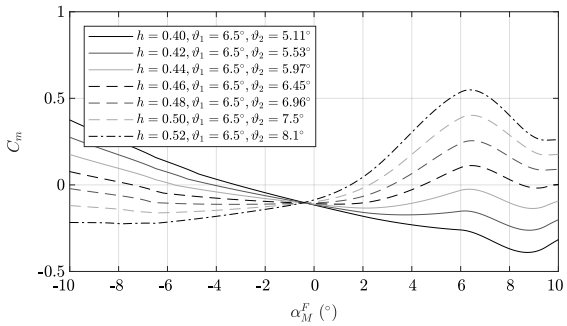

Figure 7: Longitudinal static stability analysis regarding the slope of the pitching moment coefficient C_m with respect to the angle of attack α for different center of gravity x-positions.

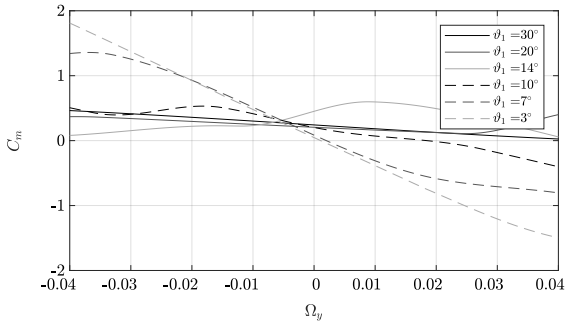

Figure 8: Longitudinal static stability analysis regarding the slope of the pitching moment coefficient C_m with respect to the dimensionless pitch rate $\Omega_y = q \cdot \bar{c}/V^A$ for different tilt angles ϑ_1 in trimmed steady horizontal flight.

Dynamic stability. While static stability describes the tendency of a system to return to the trimmed state after being perturbed, dynamic stability contains the behavior of the system over time. For the dynamic stability analysis, two root loci are used. In figure 11 the dependency of the poles to the relative cm position h is illustrated. Similarly to the longitudinal static stability analysis, according to the poles, the longitudinal motion becomes asymptotically unstable if $h \geq 0.46$ while the lateral-directional motion is unstable permanently. Moreover, figure 12 shows the poles of the tandem tiltwing during all steady-state operating points. The dutch roll motion (lateral-directional motion) is unstable once a moderate airspeed is exceeded because of the lack of a vertical stabi-

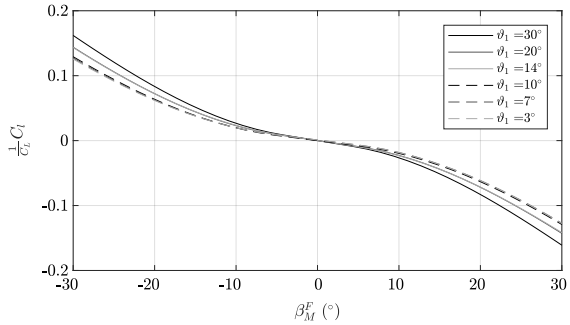

Figure 9: Lateral-directional static stability analysis regarding the slope of the rolling moment coefficient C_l with respect to the sideslip angle β for different angles of attack α.

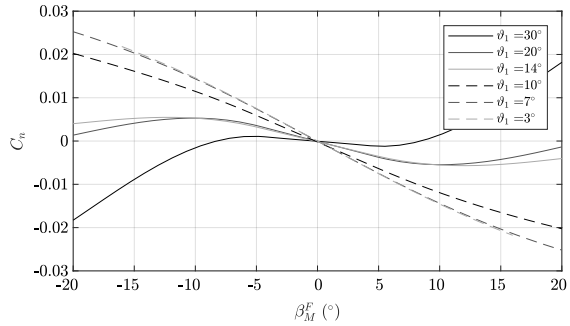

Figure 10: Lateral-directional static stability analysis regarding the slope of the yawing moment coefficient C_n with respect to the sideslip angle β for different angles of attack.

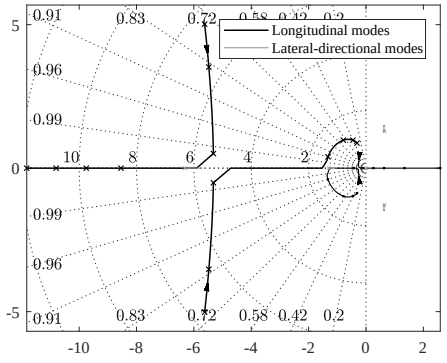

Figure 11: Stability analysis of the design point by means of a root locus varying the relative center of mass position h from $0.40 < h < 0.52$, crosses in equivalent intervals.

lizer. Regarding the longitudinal motion, the short period mode is asymptotically unstable all the time. Both longitudinal and lateral-directional motion are the most unstable for a tilt angle of $\vartheta_1 = 14°$.

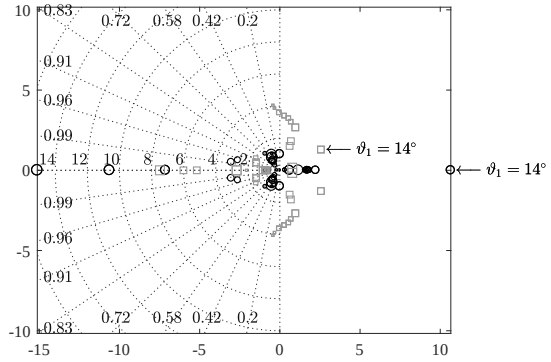

Figure 12: Stability analysis by means of a pole plot varying the steady-state operating point.

○ longitudinal motion,
□ lateral motion,
smallest markers: hover mode,
largest markers: cruise.

3.3 Control structure

The control structure, which is illustrated in figure 13, contains a gain scheduled (GS) trim command acting as feedforward as well as a GS linear quadratic regulator (LQR).

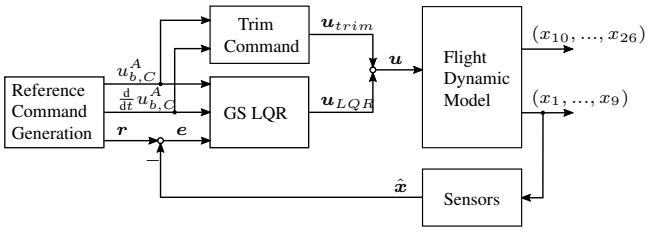

Figure 13: Diagram of the gain scheduled (GS) flight control structure.

The trim command depends on the desired airspeed as well as the desired acceleration, where the commanded acceleration is always limited to $-3\,\mathrm{m\,s^{-2}} \leq \mathrm{d}u_b^{cm/W}/\mathrm{d}t \leq 3\,\mathrm{m\,s^{-2}}$. The trim commanded tilt angles as well as the motor commands, which are normalized to $0 \leq u_{\omega_i} \leq 1$, are shown in figure 14 and 15. The trim command for the elevon deflection is always the neutral deflection.

3.4 LQR Design

According to [12] the weighting matrices $\boldsymbol{Q}$ and $\boldsymbol{R}$ for the LQR design can be chosen by determining the maximum allowed states respectively control inputs. Since the LQR is gain scheduled, the weighting matrices must be chosen sev-

http://www.imavs.org/

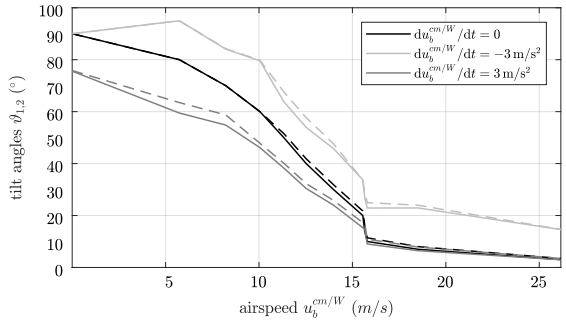

Figure 14: Tilt angle trimming (feed-forward) of the front wing (——) and the aft wing (- - -) depending on the airspeed as well as on the forward acceleration.

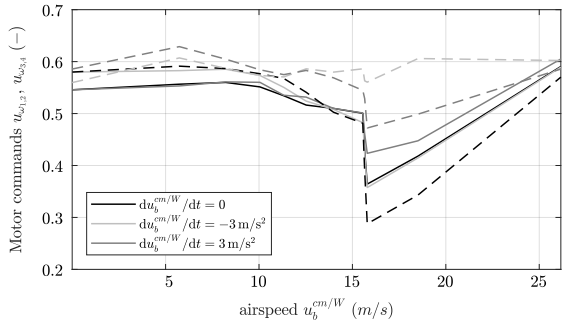

Figure 15: Motors command trimming (feed-forward) of the front motors (——) and the aft motors (- - -) depending on the airspeed as well as on the forward acceleration.

eral times (depending on the tilt angle of the front wing):

$$\boldsymbol{Q}(\vartheta_1) = \mathrm{diag}\left(\frac{1}{p_{max}^2}, \frac{1}{q_{max}^2}, \frac{1}{r_{max}^2}, \frac{1}{\Phi_{max}^2}, \frac{1}{\Theta_{max}^2}, \frac{1}{\Psi_{max}^2}, \frac{1}{{u_{b,max}^{cm/W}}^2}, \frac{1}{{v_{b,max}^{cm/e}}^2}, \frac{1}{{w_{b,max}^{cm/e}}^2}\right), \tag{2}$$

$$\boldsymbol{R}(\vartheta_1) = \mathrm{diag}\left(\frac{1}{u_{\eta_1}^2}, \frac{1}{u_{\eta_2}^2}, \frac{1}{u_{\vartheta_1}^2}, \frac{1}{u_{\vartheta_2}^2}, \frac{1}{u_{\omega_1}^2}, \frac{1}{u_{\omega_2}^2}, \frac{1}{u_{\omega_3}^2}, \frac{1}{u_{\omega_4}^2}\right). \tag{3}$$

The weighting matrices are defined for four trimpoints: $\vartheta_1 = 90°$, $\vartheta_1 = 80°$, $\vartheta_1 = 10°$, $\vartheta_1 = 7° \wedge \vartheta_1 = 3°$. Then, they are linearly interpolated in between of these points, where the weighting matrices for both cruising operating points are the same.

3.5 Closed-Loop Stability

An LQR always stabilizes the ideal linear system. Figure 16 illustrates the poles of the open-loop and the closed-loop system in its design point. It shows that the modes of the closed-loop model are well damped. However, the frequency of oscillation is increased which could increase the risk of causing structural oscillations.

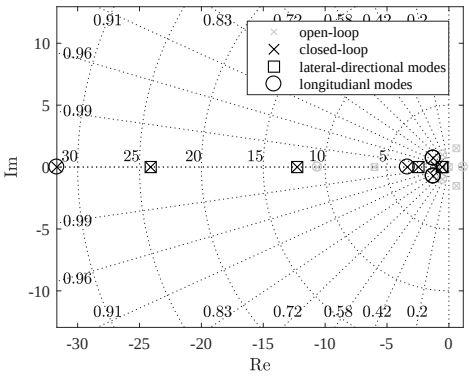

Figure 16: Pole plot of the steady-state trim point corresponding to the tilt angle $\vartheta_1 = 7°$.

3.6 Monte Carlo Robustness Analysis

The flight dynamic model contains about 100 parameters. As these parameters are more or less uncertain, the robustness of the system is investigated by varying the parameters maintaining the same controller gains. Therefore, these parameters are normally distributed by defining the expected value and the standard deviation. Then, all parameters are combined several times in order to determine the random closed-loop system dynamics. The desired outcome is the probability of failure of the real system. The necessary number of parameter combinations strongly depends on the actual probability of failure as well as the desired confidence interval [13, 14, 15].

The system stability is investigated by means of a pole distribution treating the system as a linear time-invariant system [15]. Since the tandem tiltwing model is significantly nonlinear and time-variant, the system stability is additionally investigated with aid of a dynamic maneuver covering a whole transition both forward and backwards.

Figure 17 shows the poles of 800 parameter combinations of the most unstable open-loop operating point of the tandem tiltwing and figure 18 shows the same plot for the design point. While the poles of the design point remain always stable, the most unstable open-loop operating point stays unstable in several cases. This can be explained by the high non-linearity in this area. In this operating point, the onset and ending of the wing's stall occurs (figure 9).

According to the linear-time invariant analysis, for most parameter sets, there is at least one operating point which is unstable. Mostly entirely, the unstable operating points occur at the end of the forward transition respectively at the beginning of the backwards transition because of the uncertainty of the ending and onset of the stall.

http://www.imavs.org/

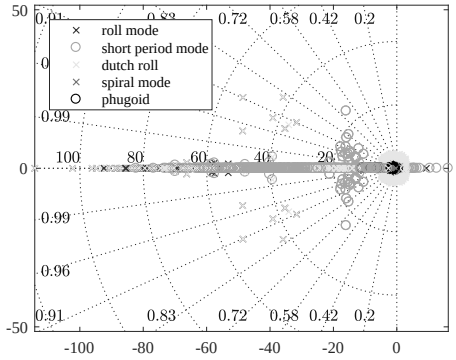

Figure 17: Linear time-invariant robustness analysis by means of a pole map of 800 parameter combinations regarding the decelerated operating point corresponding to the tilt angle of $\vartheta_1 = 14°$.

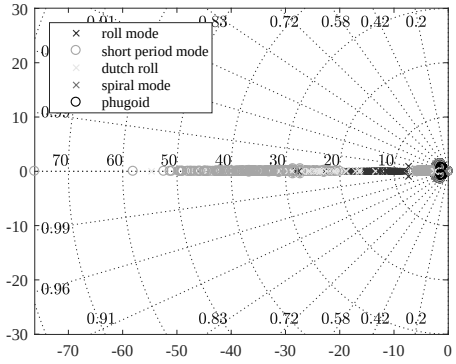

Figure 18: Linear time-invariant robustness analysis by means of a pole map of 800 parameter combinations regarding the steady-state operating point corresponding to the tilt angle of $\vartheta_1 = 7°$.

However, the dynamic maneuver robustness analysis shows that these unstable operating points are very brief. Thus, in most cases they do not lead to a failure of the system. According to the dynamic maneuver, the probability of failure can be expected to be less than $15\,\%$ within a confidence interval of $95\,\%$. All simulated failures occurred at the end of the forward transition.

4 FLIGHT TEST

In order to validate the approach of this work, a prototype of the tandem tiltwing, called Changyucopter, was constructed (figure 19).

The designed controller was implemented on a Pixhawk flight controller [16]. This flight controller contains sensors like accelerometers, gyroscopes, compasses, an airspeed sensor and a GPS receiver. The open source firmware for the Pixhawk flight controller (PX4 or ArduPilot) runs an extended Kalman filter (EKF) as state estimator. Thus, this EKF can be used for the LQR with state feedback.

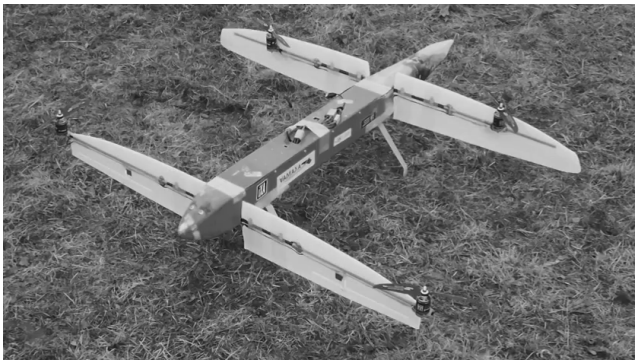

Figure 19: The first prototype of the Changyucopter tandem tiltwing.

The planned flight tests are supposed to show if the described flight dynamic model without experimental data is valid. However, possible errors of the prototype could not only be caused due to the lack of experimental data, but also due to the made assumptions. Especially the neglecting of a flexible structure and most interactions between the aerodynamic components are expected to be critical.

5 CONCLUSION

The aerodynamics of a tandem tiltwing RPAS are modeled without experimental data. Therefore, the lift and drag coefficient are interpolated with respect to the aerodynamic coefficient based on estimated characteristic points. Multiple additional aerodynamic coefficients are defined indirectly by defining moving centers of pressure. For the stability analysis and the control design, multiple steady-state, accelerated and decelerated trim points are sought and linearized. The stability analysis of the open-loop system shows that the stability derivatives are reasonable. As both the longitudinal and the lateral-directional motion are unstable, an active stabilization by a controller is crucial. The control structure consists on a gain scheduled feed-forward trim command as well as a gain scheduled LQR stabilizing the system. Since the model relies on many uncertain parameters, a Monte Carlo robustness analysis of the closed-loop system is conducted. In most trim points the system remains stable, however, there is a critical area within the transition. Instability issues occur when the tiltwing's stall starts or end because in that area the aerodynamics are highly nonlinear. Nevertheless, the instability only occurs for a short moment and the dynamic simulation shows that the RPAS quickly recovers. The flight dynamic model and the designed controller are going to be tested with a prototype of the tandem tiltwing.

http://www.imavs.org/

http://www.imavs.org/

REFERENCES

[1] Yannic Beyer. Flight control design and simulation of a tandem tilt wing RPAS. master thesis, TU Braunschweig, Institute of Flight Guidance, 2017. unpublished.

[2] Kaan Taha Öner, Ertuğrul Çetinsoy, Mustafa Ünel, Mahmut Faruk Akşit, Ilyas Kandemir, and Kayhan Gülez. Dynamic model and control of a new quadrotor unmanned aerial vehicle with tilt-wing mechanism. 2008.

[3] E. Cetinsoy, S. Dikyar, C. Hancer, K.T. Oner, E. Sirimoglu, M. Unel, and M.F. Aksit. Design and construction of a novel quad tilt-wing UAV. *Mechatronics*, 22(6):723–745, September 2012.

[4] Kaan Taha Öner, Ertuğrul Çetinsoy, EFE SIRIMOĞLU, Cevdet Hançer, Mustafa Ünel, Mahmut Faruk Akşit, Kayhan Gülez, and Ilyas Kandemir. Mathematical modeling and vertical flight control of a tilt-wing UAV. *Turkish Journal of Electrical Engineering & Computer Sciences*, 20(1):149–157, 2012.

[5] Koji Muraoka, Noriaki Okada, and Daisuke Kubo. Quad tilt wing VTOL UAV: Aerodynamic characteristics and prototype flight. In *AIAA Infotech@ Aerospace Conference and AIAA Unmanned... Unlimited Conference*, page 1834, 2009.

[6] Koji Muraoka, Noriaki Okada, Daisuke Kubo, and Masayuki Sato. Transition flight of quad tilt wing VTOL UAV. In *28th Congress of the International Council of the Aeronautical Sciences*, pages 2012–11, 2012.

[7] Samir Bouabdallah, Andre Noth, and Roland Siegwart. PID vs LQ control techniques applied to an indoor micro quadrotor. In *Intelligent Robots and Systems, 2004.(IROS 2004). Proceedings. 2004 IEEE/RSJ International Conference On*, volume 3, pages 2451–2456. IEEE, 2004.

[8] Landing Products Inc. APC Propeller Performance Data. Website, 2017. URL: `https://www.apcprop.com/Articles.asp?ID=270` [accessed on May 6, 2017].

[9] Samir Bouabdallah. *Design and Control of Quadrotors with Application to Autonomous Flying*. PhD thesis, Ecole Polytechnique Federale de Lausanne, 2007.

[10] Paul M. Rothhaar, Patrick C. Murphy, Barton J. Bacon, Irene M. Gregory, Jared A. Grauer, Ronald C. Busan, and Mark A. Croom. NASA Langley Distributed Propulsion VTOL TiltWing Aircraft Testing, Modeling, Simulation, Control, and Flight Test Development. American Institute of Aeronautics and Astronautics, June 2014.

[11] Hermann Schlichting and Erich Truckenbrodt. *Aerodynamik des Flugzeuges - Teil 2*. Springer Berlin Heidelberg, Berlin, Heidelberg, 2001.

[12] Brian L. Stevens, Frank L. Lewis, and Eric N. Johnson. *Aircraft Control and Simulation: Dynamics, Controls Design, and Autonomous Systems*. John Wiley & Sons, Hoboken, N.J, third edition edition, 2016. OCLC: ocn935444384.

[13] Robert F. Stengel and Laura R. Ray. Application of stochastic robustness to aircraft control systems. *Journal of Guidance, Control, and Dynamics*, 14(6):1251–1259, November 1991.

[14] Robert F. Stengel and L. E. Ryan. Stochastic robustness of linear time-invariant control systems. *IEEE Transactions on Automatic Control*, 36(1):82–87, 1991.

[15] Laura Ryan Ray and Robert F. Stengel. A Monte Carlo approach to the analysis of control system robustness. *Automatica*, 29(1):229–236, 1993.

[16] Lorenz Meier. Pixhawk. Website, 2017. web: `https://pixhawk.org` [accessed on September 01 2017].

APPENDIX A: MODIFIED AERODYNAMIC ANGLES

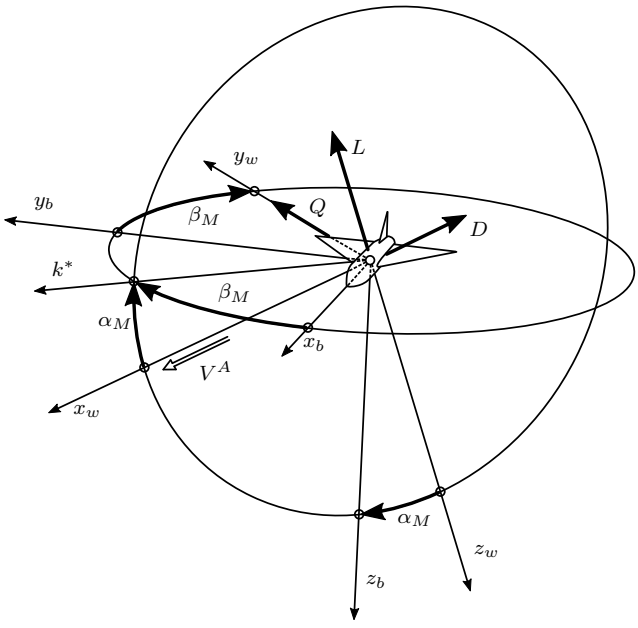

Figure 20: Definition of the modified angles α_M and β_M and the aerodynamic quantities.